Materials and Design 202 (2021) 109555

Contents lists available at ScienceDirect

Materials and Design

journal homepage: www.elsevier.com/locate/matdes

An improved electrochemical model for strain dependent electrochemical polarization and corrosion kinetics

B. Wei [a,b], D. Legut [c], S. Sun [d], H.T. Wang [e], Z.Z. Shi [f], H.J. Zhang [g,h,*], R.F. Zhang [a,b,**]

[a] School of Materials Science and Engineering, Beihang University, Beijing 100191, PR China
[b] Center for Integrated Computational Materials Engineering (International Research Institute for Multidisciplinary Science) and Key Laboratory of High-Temperature Structural Materials & Coatings Technology (Ministry of Industry and Information Technology), Beihang University, Beijing 100191, PR China
[c] IT4Innovations & Nanotechnology Center, VSB-Technical University of Ostrava, 17.listopadu 2172/15, CZ-70800, Ostrava, Czech Republic
[d] Materials Genome Institute, Shanghai University, Shanghai 200444, China
[e] CAS Key Laboratory of Nuclear Materials and Safety Assessment, Institute of Metal Research, Chinese Academy of Sciences, Shenyang 110016, China
[f] School of Materials Science and Engineering, University of Science and Technology Beijing, Beijing 100083, China
[g] National United Engineering Laboratory for Biomedical Material Modification, Dezhou, Shandong 251100, China
[h] Department of Vascular & Intervention, Tenth Peoples' Hospital of Tongji University, Shanghai 200072, China

HIGHLIGHTS

- An improved Butler-Volmer model is presented to reveal the correspondence between surface properties and corrosion behaviors under straining.
- The basal planes for pure Zn and Mg show much lower corrosion/degradation rates than the prism planes.
- Both tensile and compressive strains can promote the corrosion/degradation of Zn and Mg.

GRAPHIC ABSTRACT.

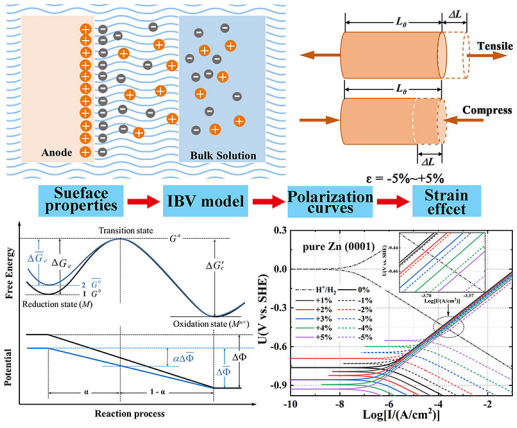

ARTICLE INFO

Article history:
Received 22 August 2020
Received in revised form 17 January 2021
Accepted 2 February 2021
Available online 4 February 2021

Keywords:
Corrosion
Butler-Volmer model
Mechanochemistry
Density functional theory

ABSTRACT

To systematically reveal the correspondence between surface properties and corrosion behaviors under mechanical conditions, an improved Butler-Volmer (IBV) electrochemical model is proposed by introducing the strain effects on electrochemical polarization through the scaled strain energy. Under mechanical straining, the three critical physical parameters i.e., surface energy, work function and strain energy, may be changed synergistically, which would consequently modify the exchange current density and equilibrium potential for the anode polarization curves. Taking two representative metals of Mg and Zn as a demonstration, it reveals that both tensile and compressive strain would contribute to the corrosion rate by lowering the activation energy barrier, in agreement with previous experimental observations. The improved model opens an alternative way to quantify the relationship between surface properties and corrosion behavior via intrinsic materials properties, which is beyond the normal design rules empirically based on either surface energy or work function alone.

* Correspondence to: H.J. Zhang, National United Engineering Laboratory for Biomedical Material Modification, Dezhou, Shandong 251100, China.
** Correspondence to: R.F. Zhang, School of Materials Science and Engineering, Beihang University, Beijing 100191, PR China.
E-mail addresses: weibo0523@buaa.edu.cn (B. Wei), dominik.legut@vsb.cz (D. Legut), mgissh@t.shu.edu.cn (S. Sun), htwang@imr.ac.cn (H.T. Wang), ryansterne@163.com (Z.Z. Shi), zhanghaijun@tongji.edu.cn (H.J. Zhang), zrf@buaa.edu.cn (R.F. Zhang).

https://doi.org/10.1016/j.matdes.2021.109555

1. Introduction

The profound effects of mechanical straining on the corrosion or degradation behavior of various metals or alloys should be taken into account [1] because mechanical straining may fundamentally modify the surface energy (γ_s), work function (Φ), and electronic polarization of metal surfaces [2,3]. Taking the biodegradable Zn and Mg alloys as an illustration, when implanted in human body as stents, they will tolerate vessel shrinkage, pulsatile pressure or other stress or strain conditions [4,5]. When under compressive strain, Jeong et al. [6] observed that for pure Mg and Mg–0.4Ca alloy under compressive strain, their cathodic reaction rates increased while the anodic reaction rates were slightly improved, resulting in a minor increase in corrosion current density (i_{corr}) and corrosion rate. A similar strain enhanced corrosion rate was also reported for the Zn–Mg–X (X = Sr, Fe) alloys by Venezuela et al. [7]. In addition, both i_{corr} and weight loss of the Mg–2.65Zn alloy was found to increase with the increasing external strain energy [8], while the corrosion rate of AM50 and AZ91D Mg–based alloys increased substantially with increasing tension loading, providing further evidence on the dependence of corrosion current and electrode potential on the applied strain or stress [9]. Although the corrosion behaviors of various metals and alloys have been widely studied in experiments, the influence of external factors on corrosion kinetic behaviors is so far not well theoretically explored due to the difficulty in appropriate modelling to characterize the complicated corrosion processes.

In terms of corrosion modelling, Ma et al. [10] proposed a scheme to calculate the corrosion kinetics by incorporating the intrinsic surface properties in framework of classical Butler-Volmer (BV) model, however it can only apply to the corrosion behavior under strain-free conditions, and thus the mechanochemical coupling effect was not considered. Besides, within the framework of classical mechanochemical model proposed by Gutman [11], Su et al. [12] explored the effect of pressure or stress on the corrosion behavior of metals, demonstrating that mechanical stress may significantly contribute the corrosion behavior of metals. However, the proposed model failed to provide a quantitative solution to bridge the correlation between corrosion behavior and surface properties during mechanical straining. Therefore, motivated by the importance and necessity of modelling to systematically reveal the correspondence between surface properties and corrosion kinetic behavior under strain conditions, an improved Butler-Volmer (IBV) electrochemical model is then proposed in the present study by simutanuously introducing the critical parameters of surface energy, work function and strain energy. Afterwards the suitability and applicability of the IBV model are thoroughly discussed by exploring the effect of mechanical straining on the electrochemical polarization and corrosion kinetics of representative metals of Mg and Zn. In short, the proposed model can provide a theoretical foundation for the study of the mechanochemical properties of materials, as well as may benefit the alloy design for certain environmental applications e.g., in biodegradable cardiovascular stent materials.

1.1. Computational methodology

The Vienna Ab initio Simulation Package (VASP) was used to perform all the DFT calculations [13], using the projector augmented wave (PAW) [14] and the Generalized Gradient Approximation (GGA) according to the Perdew-Burke-Ernzerhof (PBE) scheme [15]. The cutoff energy was set to 520 eV, the energy convergence tolerance was chosen as 10^{-5} eV/a.u., and the residual force convergence tolerance was set to 0.001 eV/Å. The three basic surface structures for Mg and Zn, i.e., (0001), $(10\bar{1}0)$ and $(11\bar{2}0)$ were modeled by nine-layer, thirteen-layer and fifteen-layer slabs, respectively, which were surrounded by the 15 Å vacuum to avoid artificial interactions between periodic images. The k-point meshes were chosen as $9 \times 9 \times 1$, $9 \times 11 \times 1$, and $9 \times 5 \times 1$ for (0001), $(10\bar{1}0)$, and $(11\bar{2}0)$, respectively.

1.2. Theoretical modelling

According to Ref. [10], the electrochemical polarization curve of the anode in a corrosive environment can be plotted in the framework of the BV model with data such as surface energy, work function, cohesion and ionization energy calculated by the first principle. As shown in Fig. 1, the basic electrochemical anodic reaction is carried out on the surface of a metal electrode, expressed as $M \leftrightarrow M^{z+} + ze^-$, where M and M^{z+} represent the initial and oxidation states of the atoms on the surface of an electrode, z is the number of electron transfers, and e^- is the electron. Recent hybrid first-principles/continuum calculations on ions adsorption to electrode surface have shown that charge transfer to oxidized species, accompanying by dehydrations of the ion occurring at a distance of less than 10 Å to electrode surface [16], leading to the generation of an energy barrier. This energy barrier arises within the Stern layer on the electrode surface as depicted in Fig. 1(a), i.e., the region between the inner and outer Helmholtz surfaces in the electrostatic double layer (EDL) [17].

In addition, Fig. 1(b) presents the energy variations and potential changes along the reaction path from M to M^{z+} during the electrochemical polarization under mechanical straining [10]. In this process, the

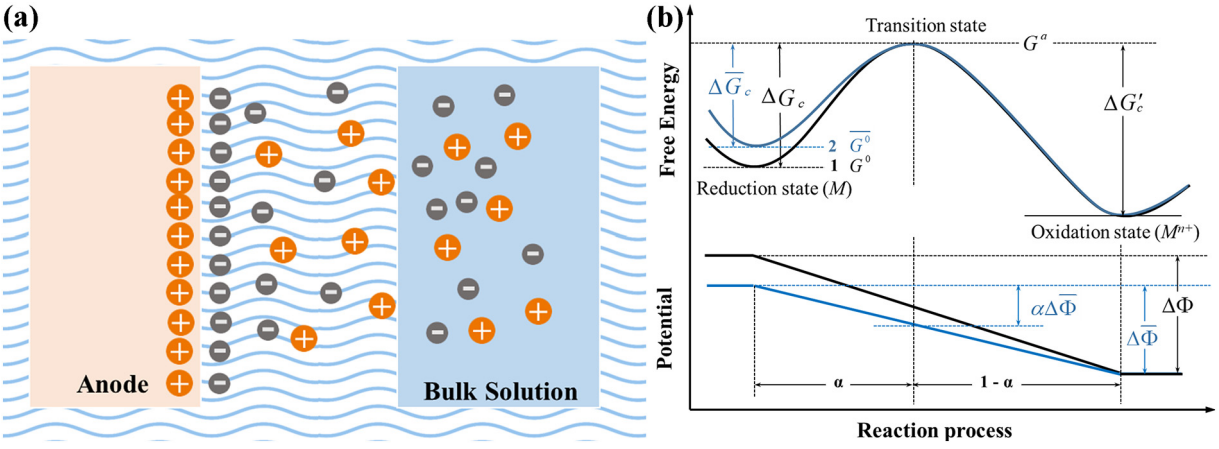

Fig. 1. (a) Schematic diagram of distribution of ions in electrical double layer (EDL). (b) Free energy change from electrode to electrolyte due to anode polarization, which includes chemical energies (namely, ΔG_c) and electrical energy ($\Delta G_e = \alpha ZF\phi_e$). When mechanical straining is applied to the electrode, a strain energy ($\Delta\overline{G}_m$) is introduced to increase the Gibbs energy of the adsorbed species, while the strain-dependent work function may modify the potential drop ($\overline{\phi_e}$) from electrode to electrolyte.

reduction state M needs to overcome the chemical activation energy ΔG_c to reach the intermediate activated state before it is finally completed to the oxidation state M^{z+}, and the traditional ΔG_c is defined as the Gibbs free energy difference between the activated state (G^a) and the initial state (G^0) when the equilibrium state is reached. Moreover, the electrostatic potential drops from electrode to the deeper electrolyte due to the screening of the EDL, as schematically shown in Fig. 1(b) for the simple physical diagram. In summary, the total change in Gibbs free energy (ΔG) during the movement of the M atom along the reaction path from the initial state to the activated state under the influence of the electrode potential consists of two components, i.e., the change in chemical energy (ΔG_c) and electric energy (ΔG_e) at ambient conditions, thus the ΔG can be defined as the electrochemical potential, i.e.,

$$\Delta G = \Delta G_c + \Delta G_e. \tag{1}$$

Here the ΔG_c may be varied under different surface states, like the occurrence of surface vacancy and/or surface adsorbed terminations [18], as well as mechanical straining, etc., thus the ΔG_c for a given material can be defined by an energy invariant (ΔG_0), plus additional surface energy contributions (ΔG_s), such as vacancy formation energy (ΔG_{sv}) and termination adsorption energy (ΔG_{st}),

$$\Delta G_c = \Delta G_0 + \Delta G_s = \Delta G_0 + \Delta G_{sv} + \Delta G_{st} + \cdots. \tag{2}$$

For a given metal under equilibrium conditions, ΔG_0 is defined as a constant that is part of the atom activation energy, independent of any specified surfaces. For simplicity, this energy can be estimated by decomposing the cohesive energy from bulk M to the free atom and its ionization energy from the free atom to ionic state, i.e., $M_{bulk} \rightarrow M_{atom} \rightarrow M^+ + e^-$ [19]. Although the precise value of ΔG_0 cannot be available from first principle calculations so far, a more realistic estimation can also be obtained by fitting the experimental polarization curves to get a consistently realistic comparison [20]. Therefore, ΔG_0 can be written as follows: $\Delta G_0 = (\mu_{M^+} - \mu_M) \times 30\%$, where μ_M represents the atomic energy for per M atom in the bulk structure and μ_{M+} represents the energy of one M^+ ion.

As regards the electric energy ΔG_e, which can be expressed as the additional energy of one surface ion transferred from the electrode surface to the electrolyte across EDL, which can be written as $\Delta G_e = \alpha ZF\phi_e$, where α, Z, F and ϕ_e represent the transfer coefficient, the number of electrons transferred, Faraday constant and the equilibrium potential, respectively. The difference between the electrostatic potential multiplied by the unit charge $e\phi_e$ can be defined as the Φ of the electrode surface, whose value is taken as a reference here for the standard potential, commonly used in other works. Specifically, Trasatti et al. [21] and Ma et al. [10] proposed an approximate expression to correlate the equilibrium potential to work function, i.e., $\phi_e = \frac{\Phi+\Delta\Phi}{e}$, where Φ represents the work function of the ideal electrode surface and $\Delta\Phi$ is a variation of Φ due to the variation of metal surface and chemical solution. Substituting the work function into the ΔG_e formula, it changes to

$$\Delta G_e = \alpha ZF\phi_e = \alpha ZF\Phi/e. \tag{3}$$

By including both energy contributions expressed by Eqs. (2) and (3) into Eq. (1), the exchange current density i_0 can be expressed as [10],

$$\begin{aligned} i_0 &= c_M nF\frac{KT}{h}\exp\left(-\frac{\Delta G}{RT}\right) \\ &= c_M nF\frac{KT}{h}\exp\left(-\frac{\Delta G_0}{RT}\right)\exp\left(-\frac{\Delta G_s}{RT}\right)\exp\left(-\frac{\alpha ZF\phi_e}{RT}\right), \end{aligned} \tag{4}$$

in which c_M is the concentration, n is the number of electrons, K is Boltzmann constant, T is temperature, h is Planck constant and R is gas constant. As known, the current density (I) in the BV model is donated as the difference between the forward current density (I_f) and the reverse current density (I_r) [12],

$$I = I_f - I_r = i_0\left[\exp\left(\frac{\alpha ZF\eta}{RT}\right) - \exp\left(-\frac{(1-\alpha)ZF\eta}{RT}\right)\right], \tag{5}$$

where $I_f = i_0\exp\left(\frac{\alpha ZF\eta}{RT}\right)$, $I_r = i_0\left[-\exp\left(-\frac{(1-\alpha)ZF\eta}{RT}\right)\right]$, where $\eta = U - U_e$ is the overpotential, which is the difference between the electrode potential U and the equilibrium electrode potential U_e. Here ϕ, ϕ_e, U and U_e are modified with respect to the Standard Hydrogen Potential (SHE) of about 4.44 V [10].

When the anode electrode is under mechanical straining, the basic physical parameters used in Eq. (4) and Eq. (5) will change accordingly, including γ_s and Φ, which would basically modify the exchange current density i_0 and equilibrium potential ϕ_e for the metal anode polarization curves. Such variations can be quantitatively calculated by first principles methods. Taking the bulk state of electrode as a reference and assuming that electrode is larger enough with its bond length being the same with its bulk counterpart, the mechanical straining may also increase the Gibbs energy of M atom at electrode surface by an additional strain dependent energetic item ΔG_m, as indicated in Fig. 1(b), and thus the change of total Gibbs energy under any straining state can be extended as,

$$\Delta\overline{G} = \Delta G_0 + \Delta\overline{G}_s + \Delta\overline{G}_e + \Delta\overline{G}_m, \tag{6}$$

where the parameters in the strain state are labeled with a bar for indicating that they are different from those in the strain-free state in Eq. (4). In which, $\Delta\overline{G}_m$ accounts for the free energy variation of reduced species M when electrode is mechanically strained (as shown in Fig. S1 (a)). Apparently, $\Delta\overline{G}_m$ is a function of the total strain energy of bulk electrode ΔG_m^b, and for simplicity, it can be adopted as the first term of Tayler series expansion of ΔG_m^b, i.e., $\Delta\overline{G}_m = \lambda\Delta G_m^b$, where λ is a scaling coefficient less than 1. Fig. S1(b) presents the dependence of $i \sim \eta$ curves on λ under mechanical straining. As shown, the value of λ can indeed affect the electrochemical polarization of electrode surface. In addition, it is worth noting that as indicated in Fig. 1(b), the appearance of mechanical straining is considered to i) not only add/modify the bulk strain energy, ii) but also contribute the modification of work function and surface energy [3], and meanwhile iii) no change is assumed for the activated state.

Considering the bulk strain energy, work function and surface energy are affected by the surface strain, the exchange current density $\bar{i}_0$ under the mechanical strain can be expressed as,

$$\begin{aligned} i_0 &= c_M nF\frac{KT}{h}\exp\left(-\frac{\Delta G}{RT}\right) \\ &= c_M nF\frac{KT}{h}\exp\left(-\frac{\Delta G_0}{RT}\right)\exp\left(-\frac{\Delta G_s}{RT}\right)\exp\left(-\frac{\Delta G_e}{RT}\right)\exp\left(-\frac{\Delta G_m}{RT}\right), \end{aligned} \tag{7}$$

Consequently, for the strained electrodes, when the potential between the electrode surface and electrolyte differs from the strain-dependent equilibrium electrode potential $\overline{U}_e$, their difference can be defined as strain-dependent potential change ΔU_e. To be noted that the appearance of ΔU_e in strain-dependent equilibrium potential $\overline{U}_e = U_e + \Delta U_e$ is ascribed to the strain-dependent variation of work function. Therefore, the current density of anodic polarization under mechanical strain ($\bar{I}$) can be expressed by the mechano-electrochemical equation proposed by Gutman [11]:

$$\begin{aligned} \bar{I} &= \bar{I}_f - \bar{I}_r \\ &= \bar{i}_0\left[\exp\left(\frac{\alpha ZF\bar{\eta}}{RT}\right)\exp\left(\frac{\Delta\overline{G}_m}{RT}\right) - \exp\left(-\frac{(1-\alpha)ZF\bar{\eta}}{RT}\right)\right]. \end{aligned} \tag{8}$$

Notably, the effect of strain on γ_s and Φ can be affected by substituting Eq. (8) for $\bar{i}_0$ and $\bar{\eta}$. On the one hand, when mechanical strain is

applied, γ_s and Φ remain constant, thus Eq. (8) becomes the original mechanical electrochemical equation proposed by Gutman [11]. On the other hand, if the bulk strain energy $\Delta\overline{G}_m$ is not considered, the equation reduces to the classical equation proposed by Ma et al. [10]. In reality, the electrode deformation cannot affect the ionic activity of the electrolyte, but can result in the parallel movement of anode polarization curves to the negative potential value since it depends on the current density of the electrode [12].

Finally, the γ_s and Φ under strain and under non-strain conditions can be calculated by,

$$\gamma_s = \frac{E_s - nE_b}{2S},\ \Phi = E_v - E_f, \tag{9}$$

where E_s is the total energy of the surface structure, n is the number of atoms contained in the surface structure, E_b is the energy of a single atom in the bulk metal structure, and S is the surface area of the surface structure; E_v is the vacuum energy and E_f is the Fermi energy.

2. Results

In general, the strained surface may possess different atomic and electronic distributions compared to the strain-free one, bringing the motivation to change the γ_s, Φ and $\Delta\overline{G}_m$ according to the applied strains. Fig. S2(a) plots the deformed structural model under uniaxial strain for the calculation of surface properties for the (0001), (10$\bar{1}$0) and (11$\bar{2}$0) surfaces of pure Zn and Mg at various strain states. The variation of the calculated $\Delta\overline{G}_m$, γ_s and Φ with the increasing of strain are shown in Fig. S2(b), Fig. 2(a) and Fig. 2(b), respectively. Some similarities and differences can be identified between Mg and Zn: 1) as shown in Fig. S2(b), the $\Delta\overline{G}_m$ of Mg and Zn show the same increasing trend within the elastic limit as the degree of tensile or compressive strain increases, providing the electrodes with enhanced Gibbs free energy; 2) the effects of uniaxial strain, biaxial strain, and hydrostatic pressure on bulk energy of different metals show a similar trend and magnitude, thus the uniaxial strain can be used to explore the strain effect on surface properties; 3) around the equilibrium state, the relationship between surface energy and strain shows an asymmetric feature (Fig. 2). Specifically, for the same surface, the sequence of surface energy variation is $\gamma_{+\varepsilon\%} > \gamma_{-\varepsilon\%} > \gamma_{0\%}$, where ε is the strain magnitude and the surface energy reaches a minimum at strain-free state, consistent with the change of bulk energy versus strain shown in Fig. 2(b), in accordance with the previous observations [22]; 4) the work functions of both Zn and Mg show a monoclinic decreasing trend with the variations of strains from compression to tension (Fig. 2), resembling the reported results by Li et al. [23] in which the Fermi energy level decreases as the bond length increases, and thus the corresponding work function decreases accordingly.

To provide a validation on the proposed IBV model, we used pure Mg and Zn as an illustration to explore their anodic polarization and corrosion kinetic properties in the corrosion-solution environments, with reference to the relevant experimental conditions being Mg in pH = 11 [24] and Zn in pH = 0 solution [25]. Herein, the cathode polarization process is $2H^+ + 2e^- = H_2$ and the U_H are −0.65 V and 0 V vs. SHE for Mg and Zn anode respectively; i_0 are 10^{-10} A/cm^2 and $10^{-7.5}$ A/cm^2 for Mg and Zn, respectively. To correspond to the kinetic processes and Tafel lines in experimental measurements, for the different crystallographic planes of Mg and Zn, the monovalent ion M^+ can generally be treated as an intermediate state for the oxidation process of one M atom [26]. Therefore, as derived from Eq. (2), we obtained ΔG_0 = 3.03 eV, 2.09 eV for Mg and Zn, respectively. Finally, other environmental parameters used in the IBV model include the room temperature of 300 K and the transient coefficients α = 0.36, 0.4 for Mg and Zn anodes, respectively, which are approximated by the previous experiments [26,27].

By incorporating the surface energy, work function, cohesion and ionization energy into the IBV model, the anodic and cathodic polarization curves may be readily calculated. Fig. 3(a) presents the flowchart for the surface-property calculation and the polarization-curve plotting in an automatic manner, and Fig. 3(b), (c) show the calculated polarization curves for different surfaces of pure Mg and Zn. It can be observed that, for pure Zn surfaces, i_{corr} are about $10^{-3.821}$ A/cm^2, $10^{-3.260}$ A/cm^2, and $10^{-3.011}$ A/cm^2 for (0001), (10$\bar{1}$0), and (11$\bar{2}$0) surfaces, respectively; while the corrosion potentials (U_{corr}) are −0.439 V, −0.501 V, and −0.535 V for (0001), (10$\bar{1}$0), and (11$\bar{2}$0) surfaces, respectively. As for pure Mg, the calculated i_{corr} are $10^{-3.681}$ A/cm^2, $10^{-3.116}$ A/cm^2, and $10^{-3.112}$ A/cm^2; U_{corr} are −1.403 V, −1.471 V, and −1.471 V for (0001), (10$\bar{1}$0), and (11$\bar{2}$0) surfaces, respectively. These results indicate that among the three surfaces for the same metal, the (0001) surface exhibits the most excellent corrosion resistance due to its lowest i_{corr} and highest U_{corr}. Moreover, the corrosion differed significantly between the basal plane ((0001) surface) and prism planes (mainly (10$\bar{1}$0) and (11$\bar{2}$0) surfaces), i.e., $U_{corr}^{(0001)} - U_{corr}^{(10\bar{1}0)}$ = 64 mV and $U_{corr}^{(0001)} - U_{corr}^{(11\bar{2}0)}$ = 94 mV, $i_{corr}^{(0001)}/i_{corr}^{(10\bar{1}0)}$ = 0.264 and $i_{corr}^{(0001)}/i_{corr}^{(11\bar{2}0)}$ = 0.15 for pure Zn; $U_{corr}^{(0001)} - U_{corr}^{(10\bar{1}0)}$ = 64 mV and $U_{corr}^{(0001)} - U_{corr}^{(11\bar{2}0)}$ = 64 mV, $i_{corr}^{(0001)}/i_{corr}^{(10\bar{1}0)}$ = 0.260 and $i_{corr}^{(0001)}/i_{corr}^{(11\bar{2}0)}$ = 0.258 for pure Mg. All these results show a good consistency to the conclusion drawn in typical experiments and calculations. For instance, the

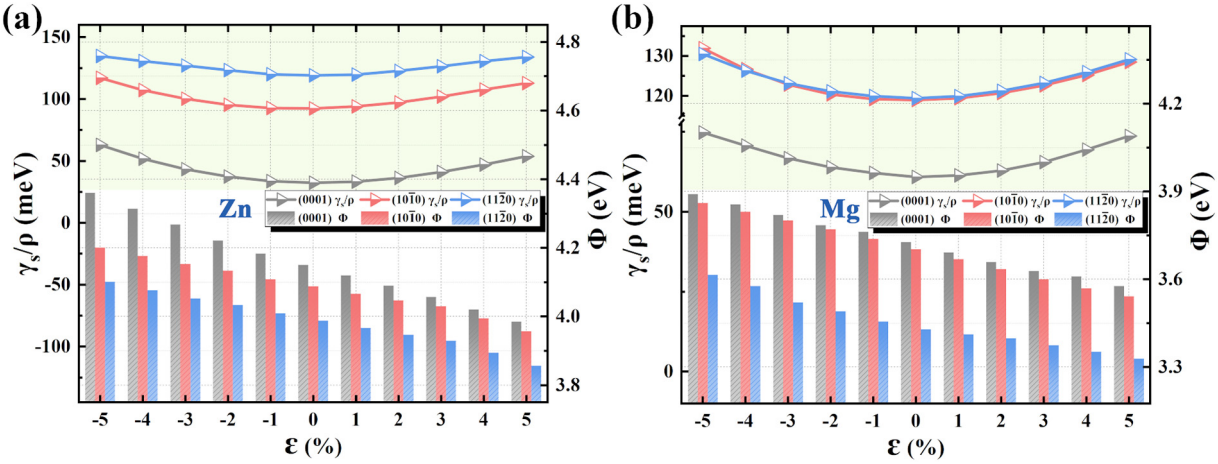

Fig. 2. The variations of surface energy density and work function vs. uniaxial strains (a) of pure Zn and (b) of pure Mg for the (0001), (10$\bar{1}$0) and (11$\bar{2}$0) surfaces.

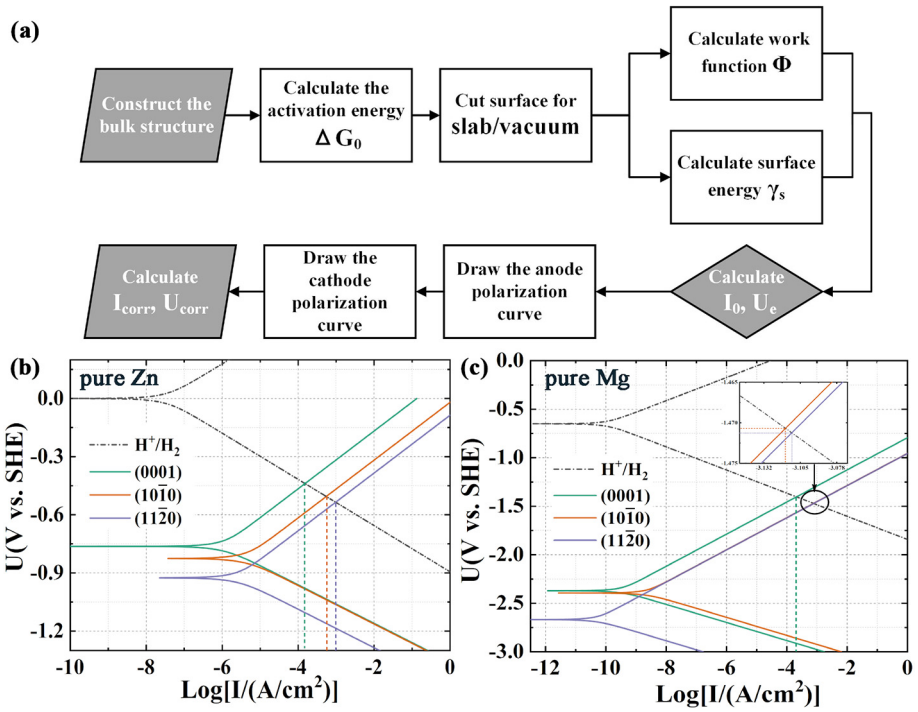

Fig. 3. (a) A flowchart to calculate the corrosion polarization curves as well as the exchange current densities and equilibrium potentials. The simulated corrosion polarization curves for the (0001), (10$\bar{1}$0) and (11$\bar{2}$0) surfaces of (b) pure Zn and (c) pure Mg. The potential (U) is defined with respect to the standard hydrogen electrode (SHE).

calculated anodic polarization curves and corrosion performance of Mg at equilibrium are in close agreement with previous calculations by Ma et al. [12], validating the present IBV model. In experiments, Ashton et al. [28] revealed that the i_{corr} of different crystallographic planes for pure Zn followed the order of (11$\bar{2}$0) > (10$\bar{1}$0) > (0001), and Song et al. [29] reported that for Mg metal, the (0001) plane exhibited more electrochemically stable and higher corrosion resistant than the (11$\bar{2}$0) and (10$\bar{1}$0) planes in 5 wt% NaCl solution, further validating the conclusion drawn in the present study.

To underline the strain effect on the anodic dissolution and corrosion behavior, Fig. 4(a) and Fig. 4(b) illustrate the simulated polarization curves of Zn (0001) and Mg (0001) surfaces with strain ranging from −5% to +5%. As can be observed, when pure Zn (0001) surface under tensile strain (+ε%), i_{corr} increases from $10^{-3.821}$ A/cm^2 (0%) to $10^{-3.620}$ A/cm^2 (+5%), resembling the case of pure Mg, i.e., i_{corr} changes from $10^{-3.681}$ A/cm^2 (0%) to $10^{-3.577}$ A/cm^2 (+5%). Additionally, under compressive strain (−ε%), i_{corr} increases to $10^{-3.545}$ A/cm^2 when strain reaches −5% for Zn (0001) surface while increases to $10^{-3.543}$ A/cm^2 for Mg (0001) surface, both higher than the increasing magnitude of i_{corr} by tensile strain. This finding exhibits good consistence to the following experimental facts, e.g., Zheng et al. [8] reported that both i_{corr} and corrosion rate of Mg–2.65Zn alloy may increase with the increasing strain, while Bonora [9] observed a similar enhanced corrosion rate for AM50 and AZ91D Mg–based alloys by tension loading. In brief, both tensile and compressive strains are shown to increase i_{corr} of Zn (0001) and Mg (0001) surfaces, yet the enhanced i_{corr} becomes more profound for compressive strain than tensile one with the same magnitude of strain.

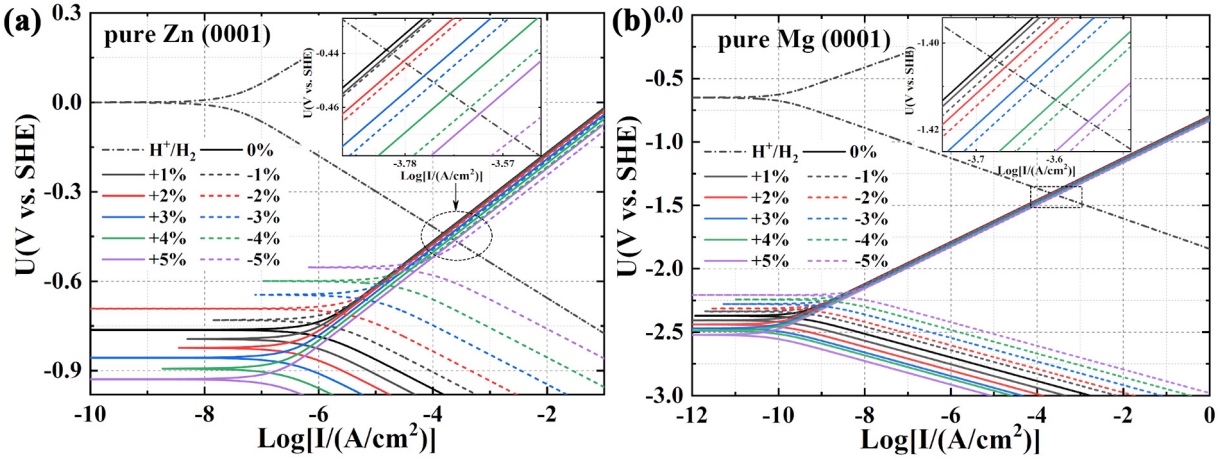

Fig. 4. The simulated corrosion polarization curves of the (0001) surfaces for (a) pure Zn and (b) pure Mg under a series of tensile or compressive strains.

3. Discussion

According to the IBV model, both surface energy and work function were used to quantify the corrosion kinetics of different materials since they were closely correlated to the current density and potentials. However, as shown in IBV model, both parameters may contribute in different manners to the corrosion resistance. To verify the effect of surface energy, work function and strain energy on the variation of corrosion polarization curves in the IBV model, Fig. 5 presents the effect of one specific parameter on the corrosion polarization curves for the same surface while keeping the other two constants. It can be seen that the same strain energy difference and surface energy density difference lead to the same variation of the exchange current density i_0 and corrosion current density i_{corr}. However, when the work function changes, both i_0 and ϕ_e change significantly while the i_{corr} and U_{corr} remain unchanged. Consequently, the changes in i_{corr} and U_{corr} are more correlated to the changes of surface energy density than the work function, i.e., the surface energy plays a more dominant role in modifying the corrosion behavior than the work function.

Moreover, it would be much necessary to provide a justification on the IBV model by comparing with some relevant BV models, i.e., the original Butler-Volmer (OBV) model [30] and modified Butler-Volmer (MBV) model [10–12]. For the three BV models, they were theoretically developed based on the kinetic theory, to show the net current as a function of an applied overpotential $\eta = U - U_e$. When $\eta = 0$, the system is in the dynamically equilibrium state with the net current is zero, at which there still exists the forward and backward currents that have the same value but with the opposite direction, i.e., the exchange current density i_0 [31]. One may notice the difference and correlation between the three models: in the present IBV model, the strain effect is considered to modify the i_0 (see Eq. (7)) and U_e via the change of two intrinsic materials parameters, i.e., γ_s and Φ, while in the MBV model, the strain (pressure) dependence is solely included in the overpotential item [32]; in OBV model, no strain effect is considered. In principle, both MBV and IBV models can be derived from each other with a certain assumption, and a consistent conclusion have been drawn on the effect of compressive strain on the corrosion behavior, i.e., it will promote the corrosion polarization process by decreasing the activation energy barrier through the bulk strain energy [12,32].

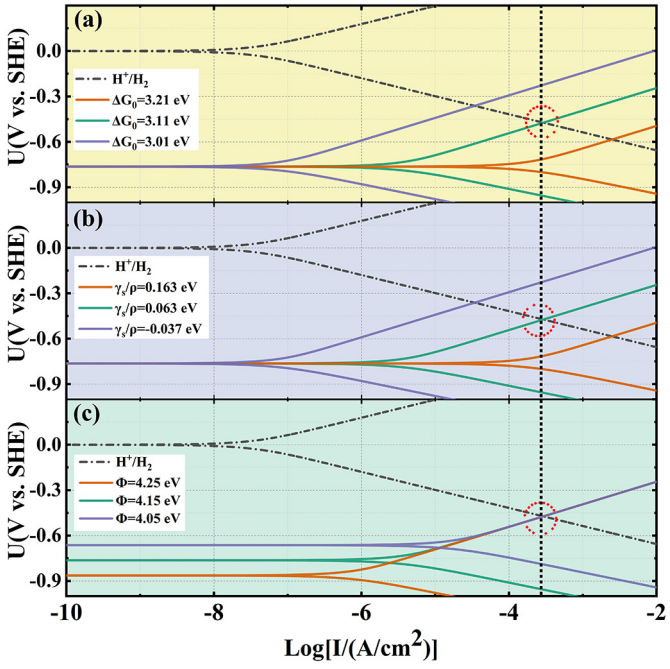

Fig. 5. The influence of mechanical straining on the surface energy, work function and strain energy which are used in IBV model: (a) the dependence of polarization curve on the strain energy, (b) the dependence of polarization curve on the surface energy density and (c) the dependence of polarization curve on the work function while keeping the other two unchanged.

In the calculation of activation energy, the electrode deformation is assumed to just affect the surface atomic activity, while the ion activity in the electrolyte will not be affected, i.e., mechanical action is extended only to solid reactants due to the increasing solid chemical potential and, consequently, the increasing reaction affinity [11]. As commented by Lu et al. [32], in the case that the net current is zero, i.e., at equilibrium or in open circuit conditions, no overpotential is present in OBV model, whereas strain-induced overpotential is clearly shown in both MBV and IBV models, i.e., $\Delta\eta = \Delta U_e = \overline{U}_e - U_e$ when strain is applied. In addition, in the actual solution environment, the metal surface is coated with kinds of particles in the solution. In the review of Zhang et al. [33], it was concluded that surface strain and adsorption can jointly affect the surface polarization. To be noted that the influence of strain on equilibrium current density i_0 was not considered in MBV and OBV models, while IBV model added this correlation. However, all these models share some common deficiencies: 1) None of these models elaborate the effect of surface defects on the corrosion reaction, such as surface vacancies and adsorbents at the metal surface; 2) For the same metal surface, the present IBV model considers merely the effect of strain on anodic dissolution, yet neglecting the variation of cathodic reactions in different environments.

4. Conclusions

An ab initio informed IBV model is developed to open an alternative way to bridge the relationship between intrinsic surface properties and corrosion behaviors under strain conditions. By means of the present IBV model, the corrosion behaviors of representative metals of Mg and Zn have been characterized under different strain conditions, demonstrating its feasibility to account for the strain dependent electrochemical polarization and corrosion kinetics. The key findings are summarized as below:

(1) The corrosion/degradation rates of the basal planes (0001) for pure Zn and Mg are much lower than that of the prism planes $(11\bar{2}0)$ and $(10\bar{1}0)$, i.e., the basal plane has a much lower corrosion current density than the prism planes, which can be attributed to the basal plane possessing the lowest surface energy, making it difficult for the initialization of corrosion.

(2) Both tensile and compressive strains are demonstrated to increase the corrosion rates of Zn and Mg metals, showing consistence with the previous experimental observations.

(3) For each metal, the compressive strain exhibits more profound effect on the corrosion performance than the same amount of tensile strain.

To be noted additionally, the present work only introduces a framework that allows users to predict the corrosion performance of pure metals during mechanical straining, while there may be more factors to be considered for a realistic quantification of metal corrosion, such as alloying elements, solution environment, particle adsorption, etc. which may be considered in the future modelling development.

Declaration of Competing Interest

There are no conflicts to declare.

Acknowledgements

This work is supported by the National Key Research and Development Program of China (No. 2017YFB0702100 and No. 2016YFC1102500), National Natural Science Foundation of China (NSFC) (No. 51672015), National Thousand Young Talents Program of

China, the Fundamental Research Funds for the Central Universities, and the ERDF in the IT4Innovations national supercomputing center - path to exascale project (CZ.02.1.01/0.0/0.0/16_013/0001791) within the OPRDE and the Large Infrastructures for Research, Experimental Development, and Innovation project "e-INFRA CZ – LM2018140" by the Ministry of Education, Youth and Sports of the Czech Republic. We thanks Prof. T. Y. Zhang, Prof. L. J. Qiao, Prof. K. W. Gao and Prof. Q. Li for their valuable comments and suggestions.

Appendix A. Supplementary data

Supplementary data to this article can be found online at https://doi.org/10.1016/j.matdes.2021.109555.

References

[1] D. Song, C. Li, N.N. Liang, F.L. Yang, J.H. Jiang, J.P. Sun, G.S. Wu, A.B. Ma, X.L. Ma, Simultaneously Improving Corrosion Resistance and Mechanical Properties of a Magnesium Alloy Via Equal-Channel Angular Pressing and Post Water Annealing, Materials & Design 166, 2019.
[2] F.L. Shi, W.P. Gao, H. Shan, F. Li, Y.L. Xiong, J.H. Peng, Q. Xiang, W.L. Chen, P. Tao, C.Y. Song, W. Shang, T. Deng, H. Zhu, H. Zhang, D.R. Yang, X.Q. Pan, J.B. Wu, Strain-induced corrosion kinetics at nanoscale are revealed in liquid: enabling control of corrosion dynamics of Electrocatalysis, Chem 6 (9) (2020) 2257–2271.
[3] S.D. Wang, W. Li, Strain-induced changes in electronic structures and work function for (001), (110) and (111) of $AlCu_3$, Phys. B Condens. Matter 406 (21) (2011) 4046–4051.
[4] J. Wang, Y. Ma, S. Guo, W. Jiang, Q. Liu, Effect of Sr on the microstructure and biodegradable behavior of mg–Zn–ca-Mn alloys for implant application, Mater. Des. 153 (2018) 308–316.
[5] S.H. Im, Y. Jung, S.H. Kim, Current status and future direction of biodegradable metallic and polymeric vascular scaffolds for next-generation stents, Acta Biomater. 60 (2017) 3–22.
[6] Y.S. Jeong, W.J. Kim, Enhancement of mechanical properties and corrosion resistance of mg–ca alloys through microstructural refinement by indirect extrusion, Corros. Sci. 82 (2014) 392–403.
[7] J. Venezuela, M.S. Dargusch, The influence of alloying and fabrication techniques on the mechanical properties, biodegradability and biocompatibility of zinc: a comprehensive review, Acta Biomater. 87 (2019) 1–40.
[8] Y. Zheng, Y. Li, J. Chen, Z. Zou, Effects of tensile and compressive deformation on corrosion behaviour of a mg–Zn alloy, Corros. Sci. 90 (2015) 445–450.
[9] P.L. Bonora, M. Andrei, A. Eliezer, E.M. Gutman, Corrosion behaviour of stressed magnesium alloys, Corros. Sci. 44 (4) (2002) 729–749.
[10] H. Ma, X.Q. Chen, R.H. Li, S.L. Wang, J.H. Dong, W. Ice, First-principles modeling of anisotropic anodic dissolution of metals and alloys in corrosive environments, Acta Mater. 130 (2017) 137–146.
[11] E.M. Gutman, Mechanochemistry of Materials, Cambridge International Science Publishing, 1998.
[12] H. Ma, X. Xiong, P. Gao, X. Li, Y. Yan, A.A. Volinsky, Y. Su, Eigenstress model for electrochemistry of solid surfaces, Sci. Rep. 6 (2016) 26897.
[13] G. Kresse, J. Furthmuller, Efficient iterative schemes for ab initio total-energy calculations using a plane-wave basis set, Phys. Rev. B Condens. Matter 54 (16) (1996) 11169–11186.
[14] G. Kresse, D. Joubert, From ultrasoft pseudopotentials to the projector augmented-wave method, Phys. Rev. B 59 (3) (1999) 1758–1775.
[15] J.P. Perdew, K. Burke, M. Ernzerhof, Generalized gradient approximation made simple, Phys. Rev. Lett. 77 (18) (1996) 3865–3868.
[16] S. Sun, L.Y. Chen, H.L. Sun, T.Y. Zhang, Adsorption and charge transfer of lithium at electrified graphene/electrolyte interface, Electrochim. Acta 259 (2018) 1089–1094.
[17] M. Khademi, D.P.J. Barz, Structure of the electrical double layer revisited: electrode capacitance in aqueous solutions, Langmuir 36 (16) (2020) 4250–4260.
[18] W.W. Xing, X.Q. Chen, Q. Xie, G. Lu, D.Z. Li, Y.Y. Li, Unified mechanism for hydrogen trapping at metal vacancies, Int. J. Hydrog. Energy 39 (21) (2014) 11321–11327.
[19] M.P. Gomes, I. Costa, N. Pebere, J.L. Rossi, B. Tribollet, V. Vivier, On the corrosion mechanism of mg investigated by electrochemical impedance spectroscopy, Electrochim. Acta 306 (2019) 61–70.
[20] W.X.S.X.C. Fu, T.Y. Yao, W.H. Hou, Physical and Chemistry, the Fifth Version Higher Education Press, Beijing, 2006.
[21] S. Trasatti, The "absolute" electrode potential—the end of the story, Electrochim. Acta 35 (1) (1990) 269–271.
[22] I.G. Shuttleworth, Non-linear modelling of the effects of strain on transition metal surfaces, Chem. Phys. Lett. 666 (2016) 51–57.
[23] W. Li, M. Cai, Y. Wang, S. Yu, Influences of tensile strain and strain rate on the electron work function of metals and alloys, Scr. Mater. 54 (5) (2006) 921–924.
[24] S. Fajardo, G.S. Frankel, Effect of impurities on the enhanced catalytic activity for hydrogen evolution in high purity magnesium, Electrochim. Acta 165 (2015) 255–267.
[25] S. Thomas, N. Birbilis, M.S. Venkatraman, I.S. Cole, Corrosion of zinc as a function of pH, Corrosion 68 (1) (2012).
[26] Y. Meng, L. Liu, D. Zhang, C. Dong, Y. Yan, A.A. Volinsky, L.N. Wang, Initial formation of corrosion products on pure zinc in saline solution, Bioactive Materials 4 (1) (2019) 87–96.
[27] V.S. Muralidharan, K.S. Rajagopalan, Kinetics and mechanism of corrosion of zinc in sodium hydroxide solutions by steady-state and transient methods, J. Electroanal. Chem. Interfacial Electrochem. 94 (1) (1978) 21–36.
[28] R.F. Ashton, M.T. Hepworth, Effect of crystal orientation on the anodic polarization and passivity of zinc, Corrosion 24 (2) (1968) 50–53.
[29] G.L. Song, R. Mishra, Z.Q. Xu, Crystallographic orientation and electrochemical activity of AZ31 mg alloy, Electrochem. Commun. 12 (8) (2010) 1009–1012.
[30] J.A.V. Butler, Studies in heterogeneous equilibria, Part II.—The kinetic interpretation of the nernst theory of electromotive force, Trans. Faraday Soc 19 (March) (1924) 729–733.
[31] A.J. Bard, L.R. Faulkner, J. Leddy, C.G. Zoski, Electrochemical methods: fundamentals and applications, wiley, New York, 1980.
[32] B. Lu, Y. Song, Q. Zhang, J. Pan, Y.T. Cheng, J. Zhang, Voltage hysteresis of lithium ion batteries caused by mechanical stress, Phys. Chem. Chem. Phys. 18 (6) (2016) 4721–4727.
[33] Y. Zhang, Mechanics of adsorption–deformation coupling in porous media, Journal of the Mechanics and Physics of Solids 114 (2018) 31–54.